nature materials

SUPPLEMENTARY INFORMATION

DOI: 10.1038/NMAT2627

Generality of shear thickening in dense suspensions

Eric Brown[1], Nicole A. Forman[2,3], Carlos S. Orellana[1], Hanjun Zhang[3], Benjamin W. Maynor[2], Douglas E. Betts[3], Joseph M. DeSimone[2,3], and Heinrich M. Jaeger[1]

[1] *James Franck Institute, The University of Chicago, Chicago, IL 60637*

[2] *Liquidia Technologies, Research Triangle Park, NC 27709*

[3] *Department of Chemistry, University of North Carolina, Chapel Hill, NC 27599*

(Dated: January 18, 2010)

I. SUPPLEMENTARY INFORMATION

A. Additional experimental details

In the rheometer the torque T on the tool and its rotation ω rate were measured and converted to a shear stress τ and a shear rate $\dot{\gamma}$. Both parallel plate and Couette geometries were used (for the parallel plate geometry $\tau = 2T/(\pi R^3)$ and $\dot{\gamma} = R\omega/d$, where R is the plate radius and d the gap size). The shear stress and shear rate describe the mechanical response in a geometry-independent form, but we do not imply or require a linear flow profile. Data for Figs. 1 and 3 were taken with increasing controlled stress to resolve the steep shear thickening, while data for Fig. 2 were taken with controlled shear rate to allow for a better fit of the Herschel-Bulkley model, Eq. 1. Care was taken that no fluid extended outside the parallel plates and the particles were confined to the space between the plates by surface tension. Samples were pre-sheared for 200 s to stresses above the shear thickening region immediately before experiments commenced after which measurements were found to be reproducible within a typical variation of about 10-20%. Measurements reported were mostly taken at ramp rates of 500 s per decade of controlled stress or shear rate. Increasing as well as decreasing ramps with different ramp rates were used to check for hysteresis, thixotropy, and transients. An example comparison of ramp rate and direction dependence is shown in Fig. I.1. Some ramp-rate independent hysteresis was observed between increasing and decreasing stress measurements. While the magnitude varied from suspension to suspension and typically about 20% of the viscosity in the shear thickening regime, the curves were never qualitatively different.

For clarity, the data shown are for one ramp direction. We checked for reversibility by shearing suspensions in the shear thickening regime and then immediately ceasing shear; the result was that the stress relaxes to the zero-shear limit within seconds. Different gap sizes between 0.5-1 mm were used to check for finite size effects. Reported experiments were done with smooth plates. Rough plates were also used in some experiments to check for slip and no significant differences were found. Reported packing fractions ϕ are based on measured particle and fluid quantities mixed together before shearing.

To observe the discontinuous viscosity curves as $\epsilon \to 0$, confinement of the sample is important. This can be achieved by either using a Couette geometry or avoiding slop in a parallel plate geometry [1, 2]. Non-density matched samples were measured in a parallel plate geometry to minimize the weight on the packing which produces a yield stress in a Couette geometry [3]. Attempts to measure shear thickening of glass spheres in mineral oil in a Couette geometry resulted in a large yield stress due to this sedimentation and no shear thickening. This observation is perfectly consistent with our conclusion that a yield stress from any source can hide shear thickening.

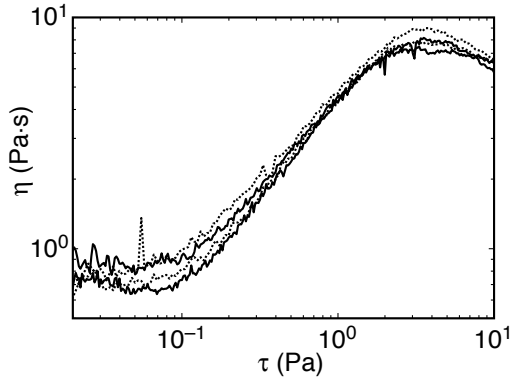

FIG. I.1: Viscosity curves showing an example of hysteresis and ramp rate dependence for 100 μm glass spheres in mineral oil at $\phi = 0.552$. Solid line: 100 measurement points per decade of stress, 10 s per point. Dotted line: 50 measurement points per decade of stress, 10 s per point. Upper curves correspond to a decreasing stress ramp. Lower curves correspond to an increasing stress ramp.

The glass spheres were obtained from MoSci corporation (Class IV). They were sieved through mesh sizes -120+170 and were measured to have a mean diameter of 89 μm with a standard deviation of 12 μm. For the surface tension experiments, the glass spheres were mixed into water after the surfactant so the total fluid volume matched that of the case without surfactant. This ensured that the surfactant diffused throughout the sample and the volume fraction did not vary between the two experiments. These measurements were done with a parallel plate setup with a 50 mm diameter rotating top plate with a 0.83 mm gap.

Cornstarch was chosen as a prototypical shear thickener for the packing fraction dependent experiments. Argo cornstarch was used at ambient conditions of 23°C and 42% humidity which included some water weight.

DOI: 10.1038/NMAT2627

The suspensions were density matched for the reported experiments so that the yield stress in this case was due to confinement [3]. For the cornstarch data shown we used a Couette geometry consisting of a 26.6 mm diameter cylinder in a cup with a gap of 1.13 mm. We found that mismatching the density for starch did not affect the critical packing fraction because in this case the hydrostatic pressure from the weight of the packing is still much lower than the yield stress above the critical packing fraction. The same behavior was also obtained in a parallel plate geometry.

For electrorheology measurements, any dielectric particle in a non-conducting fluid will work. We used hydrophobically-coated glass in mineral oil so the particle-fluid surface tension was minimized. To apply the dc electric field, 50 mm diameter parallel metal plates with a gap of 0.88 mm were used as electrodes. The reported electric field value is the applied voltage divided by the gap size. The rotating upper plate fixture made electrical contact via a wire brush. This added a constant friction corresponding to about 0.1 Pa which limited the stress resolution of those measurements. After subtracting this offset, the data in the limit of vanishing applied field matched the zero-field value measured without using the wire brush. Therefore, the stress resolution limit did not artificially set the measured onset of shear thickening.

Most magnetorheological fluids have a yield stress even in the absence of a field. To obtain a sample that showed both shear thickening and a magnetorheological response we engineered a suspension to minimize particle-fluid surface tension with particles that could be filled with magnetic material. To achieve this we used the PRINT® process. Typically, the monomer solution was prepared as follows: 0.30 g of magnetite (black iron oxide, average particle diameter = 0.2 μm, Polysciences, Inc.), 0.02 g of 1-hydroxycyclohexyl phenyl ketone (HCPK, Aldrich), and 0.01 g of fluorescein o-acrylate (Aldrich) were placed into an Eppendorf tube followed by the addition of 0.1 ml of N,N-dimethylformamide (DMF, Aldrich). The monomer mixture was then mixed thoroughly by vortex mixing to dissolve the HCPK photoinitiator and the fluorescein o-acrylate fluorophore. Lastly, 0.67 g of ethoxylated(20) trimethylolpropane triacrylate (MW = 1176 g/mol, SR415, Sartomer) was added to the monomer mixture and vortex mixed again. The resulting solution was composed of 30% (w/w) magnetite, 67% (w/w) triacrylate, 2% (w/w) HCPK, and 1% (w/w) fluorescein o-acrylate. The rod-shaped particles were then fabricated using the PRINT process, which has been described elsewhere [6, 7]. Molds for fabrication of PRINT particles were supplied by Liquidia Technologies. For the magnetorheological experiments, the particles were suspended in poly(ethylene glycol) dimethyl ether (Mn = 500 g/mol, Aldrich). These measurements were conducted in a 20 mm diameter parallel plate geometry with a gap of 0.9 mm. For imaging purposes, DyLight 549 Maleimide (MW = 1007 g/mol, Fisher) was used as the fluorophore.

B. Yield stress

The yield stress can be defined differently and thus measured in several different ways. A static or dynamic yield stress can be measured for either increasing or decreasing control ramps, respectively, and each can be done with either controlled stress or shear rate. In our experiments, each method yielded similar yield stress values. Some hysteresis was observed between the static and dynamic yield stresses, which was larger for faster ramp rates. At slower ramp rates the hysteresis loops converged to a relatively small difference (less than a factor of 2). The reported data were taken at ramp rates in this latter regime.

By defining the viscosity as $\eta \equiv \tau/\dot{\gamma}$, it is infinite below the yield stress since the shear rate is zero. Given that shear thickening requires the viscosity to increase with stress, η must first drop to finite values, so a viscosity function with a continuous first derivative necessarily displays shear thinning before entering a shear thickening region. A different value for the yield stress does not change this general behavior, but can move the onset of the shear thickening region. The shear thickening stress range can therefore depend somewhat on the yield stress definition, specifically if the lower shear thinning region is small. For the purposes of comparing shear thinning and shear thickening stresses to determine the shear thickening regime, the particular criterion for evaluating the yield stress is irrelevant as long as it is done consistently. The conclusion that the shear thickening phase boundary is determined by the shear thinning stress does not depend on which yield stress is measured or any specific form for the model. We chose the Herschel-Bulkley model with exponent 1/2 only because it fits the data well (but see below for other exponents).

C. Connection between particle interactions and macroscale rheology

The connection between field-induced interparticle attractive forces and the yield stress can be explained through electrorheology models [8]. In an applied electric field E the induced dipole moment density scales as $\beta\epsilon_0 E$ where β is an effective dielectric constant that depends on particle and fluid dielectric constants and saturates at values of order unity for all but a near-exact dielectric match. The resulting net force between neighboring particles scales as $F \sim \epsilon_0\epsilon_L\beta^2E^2a^2$ for particle diameter a and liquid dielectric constant ϵ_L. The yield stress can be obtained by dividing this attractive force by an effective particle surface area, giving a yield stress scale $\tau_y = 12\pi\epsilon_0\epsilon_L\beta^2E^2$ [8]. This result is shown in Fig. 2b and agrees with the measured yield stress at high field values. Settling becomes more important below the gravitational

stress scale $\Delta\rho g a \approx 1.5$ Pa where $\Delta\rho$ is the density difference and g is the acceleration of gravity. If the attractive stress is below this scale, particles will tend to settle at lower shear stresses rather than form chains to jam the system. This is likely the reason that the yield stress falls below the E^2 scaling at lower field values. The agreement of the yield stress with the attractive stress scale shows that the yield stress and hence the shear thickening regime can be connected to individual particle properties. It is interesting to note that this calculation did not require any specific knowledge of the flow or packing structure.

The yield stress scale could be put in terms of the attractive force divided by particle surface area, or equivalently the attractive energy per unit volume. This attractive stress scale can be calculated for other types of attractions as well to relate the yield stress to microscopic properties. For example, we can estimate the expected yield stress from other sources of interactions that might be operative between cornstarch particles. To check for this, we used optical tweezers to place two cornstarch particles next to each other in water and allowed them to diffuse. An attractive or repulsive potential can be measured by observing the probability distribution of the separation distance over time. In the tweezer experiment the resolution was about 1 pN and down to this instrumental limit no attractive or repulsive forces were observed. Dividing this value by particle surface area puts the upper limit on the yield stress due to attractions at around 10^{-2} Pa. This is consistent with the fact that we did not observe any yield stress in cornstarch suspensions down to our instrument resolution of 10^{-3} Pa at low packing fractions.

D. Approximations of the phase boundary

To understand how the lower shear thickening phase boundary is determined by the shear thinning stress, we next discuss various approximate solutions based on Eq. 3. The basic idea is as follows: Given that the shear thickening stress is independent of the strength of attractions (see Fig. 2) and described by Eq. 2, the phase boundary can be determined by measuring $\dot{\gamma}_m$, a_2 and ϵ for zero field, and then calculating $\tau_y(B)$ and $a_1(B)$ as a function of applied field. To check the feasibility of this approach, we first show that the fit parameters a_2 and ϵ are independent of the applied field. This is done by fitting the experimental data to Eq. 2 for various field values, covering a range up to 80% of the shear rate at the viscosity maximum or up to 3 Hz if there is no maximum (this covers roughly the same shear rate range). The result, shown in Fig. I.2, confirms the claim that the shear thickening stress is unaffected by (field-induced) attractions. For brevity, we will show the subsequent analysis only for the magnetorheology data but it applies for the electrorheology data as well (the ϕ dependence is more complicated because the packing fraction controls the shear thickening behavior itself in addition to tuning the yield stress).

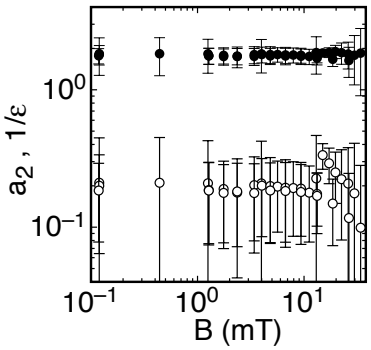

FIG. I.2: Parameter values obtained from fitting Eq. 2 to the data on shear thickening with the MR effect. (○): a_2 in units corresponding to Pa for stress and Hz for shear rate. (●): $1/\epsilon$. No resolvable trend in either parameter is found as B is varied.

The simplest approximation of the phase boundary is to assume the discontinuous limit $\epsilon = 0$. When varying the yield stress via attractive interactions, the fact that the shear thickening part of $\tau(\dot{\gamma})$ is steep means the the onset of shear thickening occurs at a nearly constant $\dot{\gamma}_m$. This allows for a simplification since we can approximate $\dot{\gamma}_m$ in Eq. 3 by its value measured for zero applied field. This gives $\tau_m = \tau_{HB}(\dot{\gamma}_m)$ indicating that the stress at the phase boundary is equal to the shear thinning stress. We evaluate Eq. 1 using fit values of $\tau_y(B)$ and $a_1(B)$ for each applied field evaluated at $\dot{\gamma}_{m,0}$, the measured onset at zero applied field. This is shown as purple symbols in Fig. I.3, along with the data from Fig. 4a. This $\epsilon = 0$ approximation underestimates the onset of shear thickening by $50 \pm 20\%$ (errors indicate a standard deviation). The fact that this approximation gives the threshold where attractions begin to move the onset and the increase in the onset with field within about a factor of 2 confirms that the phase boundary is determined by the shear thinning stress.

A better quantitative match to the lower phase boundary can be obtained by accounting for the non-zero ϵ. The orange symbols in Fig. I.3 are plotted for the same τ_y and a_1 as before but now using the measured value of $\epsilon = 0.55$. This increases the predicted τ_m by a factor of 1.5. As a result, the measured boundary is underestimated by $9 \pm 9\%$ in the low-field region and at higher fields, where attractions are reducing the shear thickening regime, by $33 \pm 20\%$. Overall, this better predicts the point where the attractions are strong enough to increase the onset of shear thickening but still underestimates the effect of attractions.

The next correction is to account for the change in $\dot{\gamma}_m$ with attractions for $\epsilon > 0$. Using techniques similar to those used in Sec. I F, an exact implicit equation can be written for $\dot{\gamma}_m$ in a form that shows how $\dot{\gamma}_m$ varies with ϵ:

DOI: 10.1038/NMAT2627

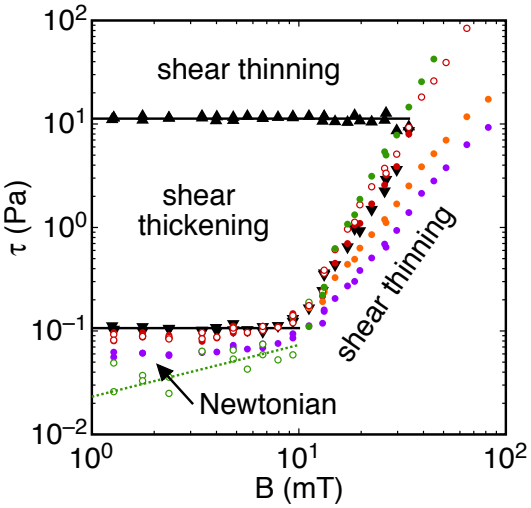

FIG. I.3: Phase diagram showing different approximations of the shear thickening phase boundary. Lower (▼) and upper (▲) boundaries of the shear thickening regime are as in Fig. 4a. Purple circles (●): estimate in the limit of $\epsilon = 0$ giving $\tau_m = \tau_{HB}(\dot{\gamma}_m)$ evaluated at $\dot{\gamma}_{m,0}$. Orange circles (●): estimate accounting for the non-zero ϵ using the measured value of $\epsilon = 0.55$ in Eq. 3. Open red circles (○): estimate further accounting for the change in $\dot{\gamma}_m$ with ϵ and B by evaluating Eq. 3 at $\dot{\gamma}_m$ calculated from Eq. I.1. Solid red circles (●): Eq. 3 at the measured $\dot{\gamma}_m$. Solid green circles (●): prediction from Eq. 3 at $\dot{\gamma}_m$ calculated from Eq. I.1 using only data obtained at $B = 0$ and the lower shear thinning regime for larger B. Open green circles (○): evaluating Eq. 3 at $\dot{\gamma}_m$ calculated from Eq. I.5 with $\alpha = 1/2$. Dotted green line: fit of the open green circles indicating the phase boundary between shear thinning and Newtonian regimes.

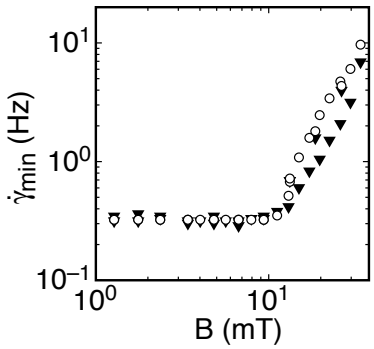

FIG. I.4: Solid triangles (▼): measured shear rate at the onset of shear thickening $\dot{\gamma}_m$. Open cirlces (○): calculated $\dot{\gamma}_m$ from Eq. I.1.

$$\dot{\gamma}_m(B)^{\frac{2-\epsilon}{2\epsilon}} = (\dot{\gamma}_{m,0})^{\frac{2-\epsilon}{2\epsilon}} + \frac{\epsilon}{2(1-\epsilon)a_2}\left[\Delta a_1(B) + \frac{2\tau_y(B)}{\sqrt{\dot{\gamma}_m(B)}}\right] \quad \text{(I.1)}$$

where $\Delta a_1(B) \equiv a_1(B) - a_1(0)$. Eq. I.1 reduces to $\dot{\gamma}_m = \dot{\gamma}_{m,0}$ for no attractions [$\Delta a_1(B) = 0$, $\tau_y(B) = 0$] as expected or for step-function stress-shear rate curves ($\epsilon = 0$) as already claimed, and it justifies the simplification $\tau_m = \tau_{HB}(\dot{\gamma}_{m,0})$ in the limit of $\epsilon = 0$. Such constant onset shear rate when the yield stress is varied in the limit of $\epsilon = 0$ contrasts with the constant onset stress when the packing fraction is varied (not including the contribution of the yield stress) [1, 4, 5].

Since Eq. I.1 is an implicit equation, it must be evaluated numerically. We note that since the yield stress is a small contribution to the overall shear thinning stress as seen in Fig. 4a, i. e. $a_1\dot{\gamma}_m^{1/2} \gg \tau_y$, the rightmost term with $\dot{\gamma}_m(B)$ in the denominator is small. Starting with the value of $\dot{\gamma}_m(B) = \dot{\gamma}_{m,0}$ on the right hand side, we can evaluate Eq. I.1 iteratively. The value of $\dot{\gamma}_m$ converges to within a few percent after only 2 iterations. Thus for a simple explicit estimate one can set $\dot{\gamma}_m(B) = \dot{\gamma}_{m,0}$ on the right side. This estimate of $\dot{\gamma}_m$ is shown in Fig. I.4 in comparison to the measured $\dot{\gamma}_m$. It is seen that the model captures the increase in $\dot{\gamma}_{min}$ with attractions, particularly the point where attractions start to increase $\dot{\gamma}_m$ which occurs at the same point the stress starts to increase due to the yield stress pushing up the onset of shear thickening. Beyond that point the model overestimates the measured values by $30 \pm 20\%$.

We now evaluate Eq. 3 using the calculated value of $\dot{\gamma}_m(B)$ from Eq. I.1, $\epsilon = 0.55$, and the fit values of $\tau_y(B)$ and $a_1(B)$. This is shown as the open red symbols in Fig. I.3 (same as in Fig. 4a) and gives the entire phase boundary within a standard deviation of 28%. For the packing fraction dependence in Fig. 4c, there is no comparable prediction for the onset shear rate because the shear thickening term varies with packing fraction. Thus the open red symbols in panel c correspond to Eq. 3 evaluated at the smallest measured onset shear rate.

A check on the validity of Eq. 3 for describing the phase boundary can be made by using the fit parameters $\tau_y(B)$ and $a_1(B)$ and $\dot{\gamma}_m(B)$ measured at the minimum of $\eta(\tau)$. This is shown as solid red symbols in Fig. I.3 (same as in Fig. 4a) which agrees with the measured phase boundary to within a standard deviation of 12%. For comparison, if we repeat measurements keeping all control parameters constant, the typical variation in the measured τ_m is 11%. Thus, the model is accurate in describing the onset of shear thickening up to the resolution of the data.

Given the assumptions that the shear thinning and thickening terms add linearly and the shear thickening term is independent of attractions, in principle we can predict the phase boundary using only the shear thickening curve at zero field and the effect of attractions on τ_{HB}. The above analysis was all done using fits of data up into the shear thickening regime. To show the predictive power of the model, we now perform the fit to the data for zero field only to obtain a_2, ϵ, and $\dot{\gamma}_{m,0}$ and keep these fixed. We then fit Eq. 2 to data for non-zero field only up to some cut-off $\dot{\gamma} < 0.3$ which is in the lower shear thinning region for data with non-zero field. This allows us to obtain τ_y and a_1. The fitting cutoff can be chosen based on the zero-field data because the

attractions always increase the onset of shear thickening. We then evaluate Eq. 3 using the fit values of τ_y and a_1, and $\dot{\gamma}_m$ from Eq. I.1. This gives the solid green symbols shown in Fig. I.3a and b.

This prediction of the phase boundary without using any data from the shear thickening regime except at zero field overestimates the phase boundary by $20 \pm 60\%$. While this agreement is not as good as when we fit the full data set, it shows that the effect of attractions on shear thickening can be predicted within about a factor of two. In the case where packing fraction is varied, the shear thickening stress itself changes; a_2 and ϵ vary with ϕ, which shifts $\dot{\gamma}_m$ without the influence of attractions. Thus either a_2 and ϵ, or $\dot{\gamma}_m$ must be obtained as a function of ϕ to determine the phase boundary.

A Newtonian regime is sometimes found before the onset of shear thickening, for example in Fig. 2a. We did not explicitly include a Newtonian term in the model. However, the generalized expression for τ_m in Eq. I.4 can apply for a Newtonian stress term when $\alpha = 1$ (see the next Section, below). The onset of shear thickening can still be expressed by τ_m in Eq. I.4 if a Newtonian stress term is added to Eq. 2, although the value of $\dot{\gamma}_{m,0}$ would generally increase. We expressed Eq. I.1 in a perturbative form rather than as a simple dependence on the fit parameters so it still applies in the case where there is a Newtonian regime whether or not it can be described by a linear addition to the stress-shear rate relation of Eq. 2. If instead Eq. I.5 is used for $\dot{\gamma}_m$ without consideration of a Newtonian regime, the phase boundary would be underestimated for weak attractions (open green symbols in Fig. I.3). Thus the difference between the open red and green circles in Fig. I.3 is due to the Newtonian regime.

For simplicity we omitted any Newtonian regime from the main paper and included it in the shear thinning regime. This does not change the conclusions but to be more general we can restate them in a way that includes the possibility of a Newtonian regime. This regime disappears for stronger attractions when the shear thinning stress overwhelms the Newtonian stress term. Thus for shear thickening to occur in general, the shear thickening stress must overcome the sum of shear thinning and Newtonian stresses. On the other hand, for attractions to affect the onset of shear thickening, they must exceed a threshold equal to the inherent shear thinning and Newtonian stresses at the onset.

E. Notes on possible mechanisms for shear thickening

The phenomenological approach presented here does not address the microscopic origin of shear thickening in suspensions, but the data put constraints on the region of validity for existing models. While hydrodynamic models have successfully described 'continuous' shear thickening which occurs at lower packing fractions and higher shear rates, they have not been able to reproduce the steep stress/shear-rate relation ($\epsilon \approx 0$) characteristic of 'discontinuous' shear thickening, instead the smallest value of ϵ allowed in those models is 1/2 [9]. Inertial granular models have a similar limitation [10]. In addition, hydrodynamic models predict that the shear thickening stress should be affected by attractions [11, 12]. However, for 'discontinuous' shear thickening this is not what we observe.

F. Derivation of Eq. 3

Here we derive an expression for the onset of shear thickening from $\tau(\dot{\gamma})$ given in Eq. 2 with a generalized Herschel-Bulkley form for the shear thinning term $\tau_{HB} = \tau_y + a_1\dot{\gamma}^{\alpha}$. The onset corresponds to the local viscosity minimum which satisfies

$$0 = \left.\frac{d\eta}{d\dot{\gamma}}\right|_{\dot{\gamma}_m} = -\frac{\tau_y}{\dot{\gamma}_m^2} + (\alpha-1)a_1\dot{\gamma}_m^{\alpha-2} + (1/\epsilon-1)a_2\dot{\gamma}_m^{1/\epsilon-2} \ . \tag{I.2}$$

Rearrangement gives

$$a_2\dot{\gamma}_m^{1/\epsilon} = \frac{\epsilon}{1-\epsilon}\left[\tau_y + (1-\alpha)a_1\dot{\gamma}_m^{\alpha}\right] \ . \tag{I.3}$$

Substituting Eq. I.3 into Eq. 2 evaluated at $\dot{\gamma}_m$ gives

$$\tau_m = \tau_{HB}(\dot{\gamma}_m) + \frac{\epsilon}{1-\epsilon}\left[\tau_y + (1-\alpha)a_1\dot{\gamma}_m^{\alpha}\right] \ . \tag{I.4}$$

Setting $\alpha = 1/2$ gives Eq. 3. This shows that in the limit of $\epsilon = 0$ the onset of shear thickening is equal to $\tau_{HB}(\dot{\gamma}_m)$ regardless of the form of the shear thinning term.

G. Derivation of Eq. I.1

Here we derive the expression for the shear rate at the onset of shear thickening $\dot{\gamma}_m$, similar to the derivation for $\tau_m(\dot{\gamma}_m)$. We rearrange Eq. I.2 to get

$$\dot{\gamma}_m^{\frac{1}{\epsilon}-\alpha} = \frac{\epsilon}{(1-\epsilon)a_2}\left[(1-\alpha)a_1 + \tau_y\dot{\gamma}_m^{-\alpha}\right] \ . \tag{I.5}$$

To put this in the form of Eq. I.1 to directly describe the perturbation in $\dot{\gamma}_m$ with an additional shear thinning term, we evaluate this for zero additional attractions to obtain

$$\dot{\gamma}_{m,0}^{\frac{1}{\epsilon}-\alpha} = \frac{\epsilon}{(1-\epsilon)a_2}(1-\alpha)\left(a_1 - \Delta a_1\right) \tag{I.6}$$

where $\Delta a_1 \equiv a_1 - a_{1,0}$ and $a_{1,0}$ is the value of a_1 for the unperturbed state without the additional shear thinning term. Substituting this back in to Eq. I.5 to eliminate a_1 results in

DOI: 10.1038/NMAT2627

We evaluate this at $\alpha = 1/2$ to obtain Eq. I.1.

$$\dot{\gamma}_m^{\frac{1}{\epsilon}-\alpha} = \dot{\gamma}_{m,0}^{\frac{1}{\epsilon}-\alpha} + \frac{\epsilon}{(1-\epsilon)a_2}\left[(1-\alpha)\Delta a_1 + \tau_y \gamma_m^{-\alpha}\right] \ . \quad \text{(I.7)}$$

[1] Brown, E., Jaeger, H. M. *Dynamic jamming point for shear thickening suspensions.* Phys. Rev. Lett. **103**, 086001-1–4 (2009).

[2] Fall, A., Huang, N., Bertrand, F., Ovarlez, G., & Bonn, D. *Shear thickening of cornstarch suspensions as a reentrant jamming transition.* Phys. Rev. Lett. **100**, 018301-1–4 (2008).

[3] Fall, A., Bertrand, F., Ovarlez, G., & Bonn, D. *Yield stress and shear banding in granular suspensions.* Phys. Rev. Lett. **103**, 178301-1–4 (2009).

[4] Maranzano, B.J. & Wagner, N.J. *The effects of particle size on reversible shear thickening of concentrated colloidal suspensions.* J. Chem. Phys. **114**, 10514 - 10527(2001).

[5] Egres, R.G. & Wagner, N.J. *The rheology and microstructure of acicular precipated calcium carbonate colloidal suspensions through the shear thickening transition.* J. Rheol. **49**, 719-746 (2005).

[6] Rolland, J.P, Maynor, B.W., Euliss, L.E., Exner, A.E., Denison, G. M., DeSimone, J.M. *Direct Fabrication and Harvesting of Monodisperse, Shape-Specific Nanobomaterials.* J. Am. Chem. Soc. **127**,10096-10100 (2005).

[7] Herlihy, K.P., Nunes, J., & DeSimone, J.M. *Electrically Driven Alignment and Crystallization of Unique Anisotropic Polymer Particles.* Langmuir **24**, 8421-8426 (2008).

[8] Zukoski, C.F. *Material properties and the electrorheological response.* Annu. Rev. Mater. Sci. **23**, 45-78 (1993).

[9] Bergenholtz, J., Brady, J.F. & Vivic, M. *The non-Newtonian rheology of dilute colloidal suspensions.* J. Fluid Mech. **456**, 239-275 (2002).

[10] Bagnold, R.A. *Experiments on a gravity-free dispersion of large solid spheres in a Newtonian fluid under shear.* Proc. Royal Soc. London. Series A, Mathematical and Physical Sciences, No. 1160, 49-63 (1954).

[11] Shenoy, S.S., Wagner, N.J. & Bender, J.W. *E-FiRST: Electric field responsive shear thickening fluids.* Rheol Acta **42**, 287-294 (2003).

[12] Gopalakrishnan, V, Zukoski, C.F. *Effect of attractions on shear thickening in dense suspensions.* J. Rheol. **48** , 1321-1344 (2004).